frontiers in Chemical Engineering

ORIGINAL RESEARCH
published: 21 September 2021
doi: 10.3389/fceng.2021.723429

Rheological and Printability Assessments on Biomaterial Inks of Nanocellulose/Photo-Crosslinkable Biopolymer in Light-Aided 3D Printing

*Qingbo Wang[1], Oskar Backman[1], Markus Nuopponen[2], Chunlin Xu[1] and Xiaoju Wang[1,3]**

[1]*Laboratory of Natural Materials Technology, Faculty of Science and Engineering, Åbo Akademi University, Turku, Finland,* [2]*UPM-Kymmene Corporation, Biomedicals, Helsinki, Finland,* [3]*Pharmaceutical Sciences Laboratory, Faculty of Science and Engineering, Åbo Akademi University, Turku, Finland*

Biomaterial inks based on cellulose nanofibers (CNFs) and photo-crosslinkable biopolymers have great potential as a high-performance ink system in light-aided, hydrogel extrusion-based 3D bioprinting. However, the colloidal stability of surface charged nanofibrils is susceptible to mono-cations in physiological buffers, which complexes the application scenarios of these systems in formulating cell-laden bioinks. In this study, biomaterial inks formulated by neutral and negatively surface charged CNFs (GrowInk-N and GrowInk-T) and photo-crosslinkable biopolymers (gelatin methacryloyl (GelMA) and methacrylated galactoglucomannan (GGMMA)) were prepared with Milli-Q water or PBS buffer. Quantitative rheological measurements were performed on the ink formulations to characterize their shear flow recovery behavior and to understand the intermolecular interactions between the CNFs of different kinds with GGMMA or GelMA. Meanwhile, printability assessments, including filament extrudability and shape fidelity of the printed scaffold under varying printing conditions, were carried out to optimize the printing process. Our study provides extensive supporting information for further developing these nanocellulose-based systems into photo-crosslinkable bioinks in the service of cell-laden 3D bioprinting.

Keywords: cellulose nanofibrils, photo-crosslinkable biopolymer, light-aided extrusion-based 3D printing, printability assessment, rheology

OPEN ACCESS

Edited by:
Per Stenius,
Aalto University, Finland

Reviewed by:
Liangliang Lin,
Jiangnan University, China
Arne Reinsdorf,
Evonik Industries, Germany

****Correspondence:***
Xiaoju Wang
xiaoju.wang@abo.fi

Specialty section:
This article was submitted to Chemical Reaction Engineering, a section of the journal Frontiers in Chemical Engineering

Received: *10 June 2021*
Accepted: *29 July 2021*
Published: *21 September 2021*

Citation:
Wang Q, Backman O, Nuopponen M, Xu C and Wang X (2021) Rheological and Printability Assessments on Biomaterial Inks of Nanocellulose/Photo-Crosslinkable Biopolymer in Light-Aided 3D Printing. Front. Chem. Eng. 3:723429. doi: 10.3389/fceng.2021.723429

INTRODUCTION

In the research context of regenerative medicine and tissue engineering, three-dimensional (3D) printing techniques are advantageous to fabricate the biomimetic hydrogels of site-specific geometry and with a complex structure (Hinton et al., 2015). From the hydrogel fabrication point of view, these additive manufacturing methods highlight the convenient workability of automation, reproducibility, and, in particular, a personalized design aided by a digital model (Gillispie et al., 2020). An extrusion-based 3D printing system with a piston-derived syringe and microscale needle is mostly adopted among the 3D printing methods that are suitable for hydrogel printing (Kang et al., 2016; Gillispie et al., 2020). Furthermore, a variety of ink formulations consisting of high concentration water-soluble polymers such as alginate, gelatin, and collagen have been developed for the printing process (Rhee et al., 2016; Lewis et al., 2018; Yang et al., 2018). Recently, attributed to structural similarity to extracellular matrix, low cytotoxicity, and desirable

rheological properties, the gel-like cellulose nanofibrils (CNFs) have attracted increasing attention as an ingredient when formulating the bio(material) inks for hydrogel extrusion-based 3D bioprinting (Shin et al., 2017; Heggset et al., 2019). To accurately reproduce the structure of the digital model and to achieve adequate shape fidelity are challenging factors in the scenarios of extrusion-based 3D printing because of the soft nature of the CNFs-based hydrogels, which typically have a water content greater than 95%. CNFs can be either printed as a monocomponent hydrogel as a platform biomaterial (Ajdary et al., 2019) or more often in binary ink formulations with other biopolymers, such as gelatin and alginate (Markstedt et al., 2015; Ojansivu et al., 2019), where CNFs are more often seen as a rheological modifier to facilitate the extrudability/printability and to promote the shape fidelity performance of the formulated bioink. In order to improve the ink fidelity, different crosslinking strategies such as ionic crosslinking (Rees et al., 2015), thermal crosslinking (Xu et al., 2018b), enzymatic crosslinking (Huang et al., 2020), and photo-crosslinking (Ma et al., 2020) were implemented in previous studies. In an up-to-date research context, light-aided 3D bioprinting is a prevailing approach for biofabrication. Here, the hydrogel bioink that contains the photo-crosslinkable biopolymer such as gelatin methacryloyl (GelMA) or hyaluronic acid methacrylate (HAMA) can be rapidly cross-linked into a covalent network *via* free-radical chain polymerization upon UV irradiation. This process can take place *in situ* either right after the ink being extruded through the nozzle on the collecting board or while the ink is still being run through the nozzle of a special type that allows UV penetration (Lim et al., 2020). Attributed to beneficial biological properties, GelMA, a derivative of gelatin that still preserves the residual cell attachment motif from native ECM, has been widely used in such types of photo-crosslinkable bioink formulations. Xu et al. (2019a) reported 3D printing of a binary biomaterial ink of TEMPO-mediated oxidized CNFs and low-concentration GelMA. The printed hydrogels showed mechanical strength in the range of 2.5–5 kPa and promoted the proliferation of fibroblasts. Adjusting the printed hydrogels' mechanical properties enables them to mimic biomechanical properties of natural biological tissues that could regulate the fate of the attached cells (Engler et al., 2006; O'Brien, 2011). Xu et al. (2019b) developed a wood-derived biomaterial ink composed of TEMPO-mediated oxidized CNFs and galactoglucomannan methacrylates (GGMMAs) with a different substitution degree of methacrylates. The results showed that the fabricated hydrogels displayed a broad and tunable mechanical strength ranging from 2.5 to 22.5 kPa. Fan et al. (2020) incorporated 10 wt% of cellulose nanocrystals into GelMA/HAMA to reinforce the printed hydrogels' mechanical property, which serves as a structure-supporting material in a hybrid printing strategy (Fan et al., 2020).

In hydrogel extrusion-based 3D printing, the ink fidelity of the CNFs/photo-crosslinkable biopolymer inks is largely determined by the rheological properties of the hydrogel ink, which are intrinsically dictated not only by the physiochemical properties of CNFs, such as nanodimension and surface charge density, but also by interactions between CNFs and photo-crosslinkable polymers (Hubbe et al., 2017; Xu et al., 2019b). CNFs prepared solely by mechanical defibrillation have a relatively larger dimension, and the colloidal stability of the dispersion is mainly attributed to the physical entanglement between CNFs with a high aspect ratio (Nechyporchuk et al., 2016). As there is no oxidation involved in the preparation process, the mechanically defibrillated CNFs typically have a rather low negative surface charge density. This makes this type of CNFs insensitive to the ionic strength of metal ions in terms of the microstructure stability within a hydrogel, which is a preferred scenario in cell-laden 3D bioprinting when applied to formulating bioinks upon mixing with cell-containing physiological buffers, e.g., phosphate buffered saline (PBS). CNFs can also be prepared by mechanical defibrillation in combination with such a pretreatment as TEMPO-mediated oxidation. Owing to the small nanodimension of fibrils and the negative surface charge induced by the oxidation reaction, the TEMPO-oxidized CNFs possess a higher water retention ability and are more transparent when forming hydrogels (Benhamou et al., 2014). Hence, they are accepted as a generic type of biomaterial in supporting the suspended 3D cell culture as well as in constructing biomedical hydrogels (Lou et al., 2014). Furthermore, quite a few studies have reported the development of biomaterial inks with the TEMPO-oxidized CNFs for 3D printing (Xu et al., 2018a; Li et al., 2018). It is worth noting that the colloidal stability of TEMPO-oxidized CNFs dispersion dispersion is sensitive to monovalent cations as the nanofibrils are stabilized by the electronic repulsion between the negatively charged nanofibrils (Fukuzumi et al., 2014; Levanič et al., 2020). Eventually, this aspect challenges its application in cell-laden 3D bioprinting as the monovalent cations when introduced with the PBS buffer in cell mixing can cause flocculation of TEMPO-oxidized CNFs, and it further hinders its printability.

In the current study, biomaterial inks engaging mechanically defibrillated CNFs or TEMPO-oxidized CNFs with GelMA and GGMMA (with or without PBS buffer) were formulated, and the ink printability in light-aided extrusion-based 3D printing was investigated. The influence of PBS buffer on the formulated inks was analyzed by quantitatively characterizing the rheological properties and photo-crosslinking kinetics. In addition, the printability of the formulated inks was evaluated by a series of tests, including single filament extrusion uniformity and the filament fusion test in multi-layer cross-hatch grids under different printing conditions. We have aimed to optimize and validate the printability of these UV-curable and CNFs-based biomaterial inks and to provide principal information for future use of these inks in cell-laden 3D bioprinting aided by photo-curing.

MATERIALS AND METHODS

Materials

Mechanically defibrillated CNFs (GrowInk-N, 2.5 wt%) and TEMPO-oxidized CNFs (GrowInk-T, 2 wt%) were donated by UPM Biomedicals. Phosphate buffered saline tablets (PBS, Biotechnology grade) were purchased from VWR Life Science. Lithium phenyl-2,4,6-trimethylbenzoylphosphinate (LAP) and

deuterium oxide (D_2O) containing 0.75 wt% 3-(trimethylsilyl) propionic-2,2,3,3-d_4 acid (TMSP) were purchased from Sigma-Aldrich. Dulbecco's modified eagle's medium (DMEM, high glucose) was purchased from Biowest. GelMA was purchased from ALLEVI (Philadelphia, United States). GGMMA was in-house synthesized following a reported method (Xu et al., 2019b).

Method

Characterization of the Ink Ingredients

The nanomorphologies of CNFs in GrowInk-N and GrowInk-T were obtained via a transmission electron microscope (TEM, JEM-1400 PLUS). The charge density of GrowInk-N and GrowInk-T was determined by the potentiometric titration method reported by Chinga-Carrasco et al. (2014). The degree of methacryloylation (DM) of GGMMA (0.862 mmol/ g) and GelMA (0.463 mmol/ g) was determined by ^{1}H NMR spectroscopy using a method reported by Claaßen et al. (2018). The results were displayed in **Figure 1**.

Ink Formulation

The ink formulations in this study are listed in **Supplementary Table S1**. Briefly, the inks were prepared by diluting GrowInk-N (2.5 wt%) and GrowInk-T (2 wt%) with PBS buffer or Milli-Q water. Then, the lyophilized powder of GGMMA or GelMA was mixed with diluted GrowInk-N or GrowInk-T at 50°C using a vortex mixer. LAP was selected as the photoinitiator and added to each ink to make a final concentration of 0.1 wt%. The inks were stored in a cold and dark place for 24 h before measurement.

Rheological Measurements

Rheological properties of the inks were measured by using an MCR 702 MultiDrive rheometer (Anton Paar GmbH) with a PP25 parallel-plate at 25°C (diameter: 25 mm and gap: 0.5 mm). Viscosity curves were obtained through shear flow measurement with a shear rate ramp-up and ramp-down of 0.01–1000 s^{-1} in logarithmic scale with 1 s per data point. Amplitude sweep was performed with a strain range from 0.01 to 500% at a constant frequency of 1 Hz at 25°C. The data acquisition time was 10 s per data point. The thixotropic behavior of the inks was analyzed by shearing the sample at 0.1 s^{-1} for 60 s, followed by shearing at 700 s^{-1} for 10 s and then at 0.1 s^{-1} for 60 s. The samples were pre-sheared at 1 s^{-1} for 20 s and equilibrated for 60 s before all measurements were taken. Photo-crosslinking kinetics of the inks were measured at a constant strain and frequency of 0.1% and 1 Hz, respectively. The samples were irradiated with UV (bluepoint 4 ecocure UV lamp, The Hönle Group, Germany) after 1 min, and the storage modulus was registered.

Printability Assessment

Printability assessment of the inks was performed at room temperature with a 3D bioprinter from ROKIT INVIVO (ROKIT, South Korea), equipped with a piston-driven extrusion nozzle. The inks were loaded into a 3 ml syringe with a steel needle gauge of 25 GA (inner diameter: 0.25 mm) for printability assessment. A UV-LED spotlight (wavelength: 365 nm and energy output: 10 mW/ cm^2; bluepoint LED eco, The Hönle Group, Germany) was applied for photo-crosslinking during the printing process. The schematic image of the 3D bioprinter and the hydrogel extrusion-based printing process is displayed in **Supplementary Figure S1**.

Uniformity Ratio Measurement

The uniformity analysis of the printed filaments was followed by a reported method with modifications (Gao et al., 2018). Briefly, three filaments were printed on a microscopic slide under a controlled input flow rate and printing speed for each ink. The input flow rate was set at 100, 110, or 120%, and the printing speed was set at 4, 8, 12, 16, or 20 mm/ s. The shape of each filament was recorded by a digital microscope (Nikon ECLIPSE E200 with a Nikon DIGITAL SIGHT DS-US camera). The filaments' outline length on both sides and diameter were manually measured by ImageJ software. The uniformity ratio was determined by the ratio between the length of the filament outline and the filament itself.

Semi-Quantification of Printability

10-layer cross-hatch scaffolds of each ink with five vertical and five horizontal lines with a span width of 1.25 mm were printed to evaluate the printability. The layer height was set at 0.07, 0.08, or 0.09 mm, and the input flow rate was set at 100, 110, or 120%. The printed scaffold was washed and soaked in PBS buffer for 24 h after printing, and then the photos of the printed scaffold were taken by using a microscope. The printability value (Pr) and diffusion rate value (Dr) were adopted for printability evaluation (Ouyang et al., 2016; Habib et al., 2018). The Pr value is defined as in **Eq. 1** by comparing the circularity of a square (π/4) with the outcome pores,

$$P_r = \frac{L^2}{16A} \tag{1}$$

where L and A are the perimeter and area of the outcome pores, respectively.

The Dr value is defined as in **Eq. 2** by comparing the difference between the actual area of outcome pores and the theoretical area defined from the line spacing and nozzle size,

$$D_r = \frac{A_t - A_a}{A_t} \tag{2}$$

where A_t and A_a mean the theoretical area and actual area, respectively. The perimeter and area of the pores were manually measured by ImageJ software.

Scaffold Stability

36-layer cross-hatch scaffolds with a layer height of 0.09 mm of each ink were printed for scaffold stability analysis. The printed scaffolds were incubated in PBS buffer and DMEM for 7 days.

Mechanical Test

The mechanical property of the cast hydrogel discs (diameter: 8 mm and height: 4.5 mm) was measured with an MCR 702 MultiDrive rheometer under the compression mode. The compression speed and displacement were set at 0.1 mm/ s and 3.5 mm, respectively. The compressive Young's modulus was calculated according to a reported method (Xu et al., 2019b).

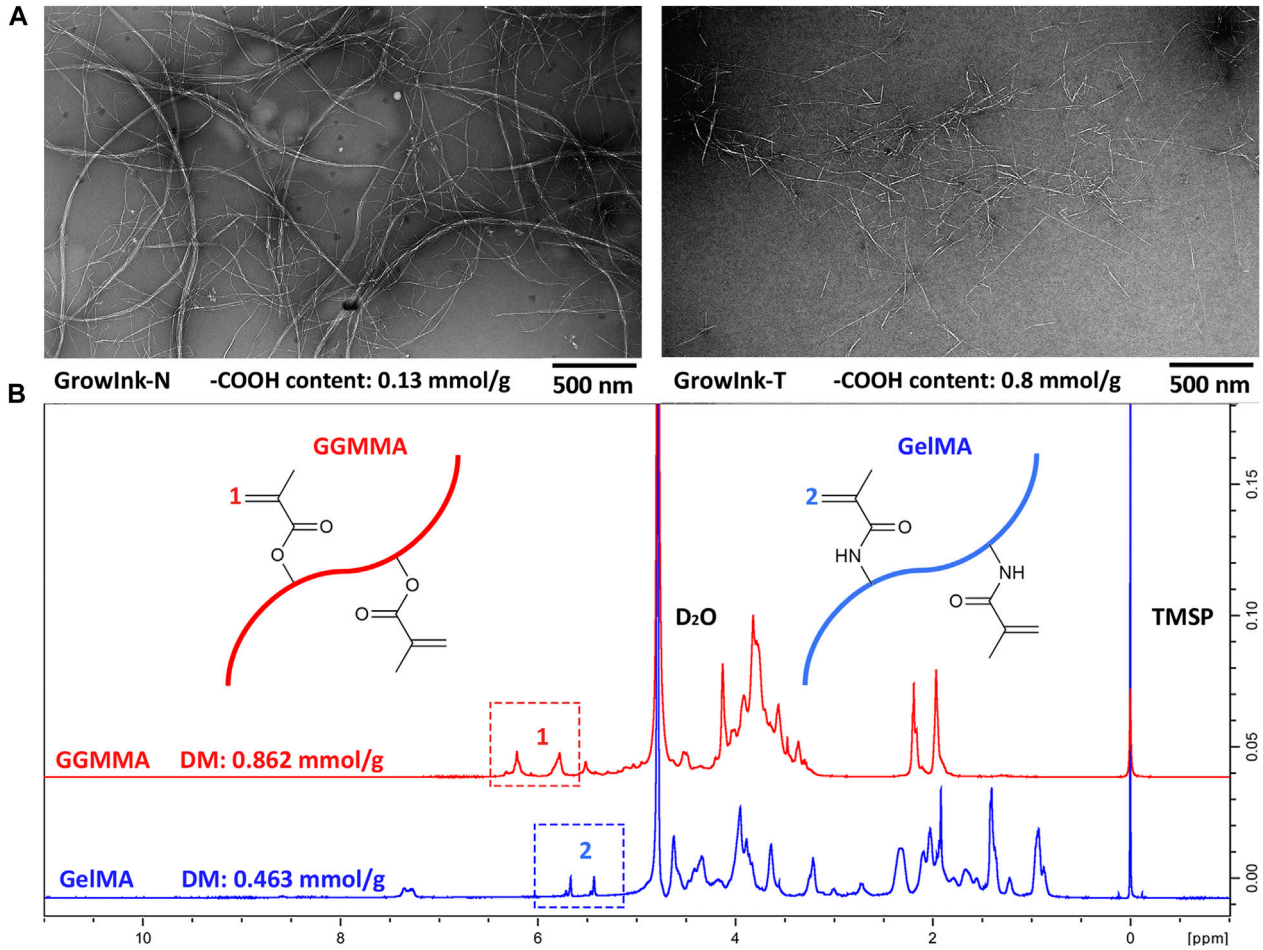

FIGURE 1 | (A) TEM images of GrowInk-N and GrowInk-T and **(B)** ^{1}H NMR spectra of GGMMA and GelMA.

RESULTS AND DISCUSSION

Rheological Property

Rheological studies were carried out to understand the flow behavior and viscoelastic properties of the CNFs-based inks. The viscosity of each formulated ink as a function of the shear rate was recorded in ramp-up and ramp-down experiments, as displayed in **Figure 2**. The shear-thinning response upon shearing, a prerequisite ink property for extrusion-based 3D printing, could be observed in all formulated inks. For inks with the same composition, their viscosity increases with the increase in CNF content. As shown in **Figures 2A and B**, GrowInk-N-PBS displayed a higher viscosity and hysteresis behavior than GrowInk-N-water. This is mainly due to the moderate electrostatic screening effect caused by monocations in PBS buffer, which reduces the distance between CNFs (Saarikoski et al., 2012). The CNFs are more likely to aggregate into flocs, which, thus, increases the ink's viscosity at rest or at a low shear rate. However, the flocs are likely to be dissociated into nanofibrils at a high shear rate and difficult to recover immediately, leading to hysteresis behavior (Oh et al., 2020). Meanwhile, the flocs will also form an uneven microstructure of the ink, which is not conducive to its printability. However, the hysteresis behavior of GrowInk-N-PBS disappeared after the incorporation of GGMMA, as shown in **Figure 2F**. This might be attributed to the steric stabilization by the GGMMA, which is a high-molecular-weight and water-soluble heteropolysaccharide that has an intrinsic affinity/adsorption to the nanocellulose surface via hydrogen bonding (Xu et al., 2019b). It is inferred that the adsorbed GGMMA tends to prevent the closely approaching CNFs from aggregating into flocs, thus consequently preventing the hysteresis behavior and uneven microstructure of the GrowInk-N-PBS inks (Winter et al., 2010; Hubbe et al., 2017). On the other hand, the electrostatic screening effect in GrowInk-N-GGMMA-PBS inks still exists, leading to a higher viscosity than the GrowInk-N-GGMMA-water inks, as shown in **Figure 2E**. A significant increase in viscosity was observed in **Figures 2I and J** by introducing 5% of GelMA to GrowInk-N-GelMA–based inks. Moreover, GelMA also showed the ability to reduce the hysteresis behavior in GrowInk-N-GelMA-PBS inks, as shown in **Figure 2J**. Incorporation of GGMMA or GelMA with GrowInk-N would

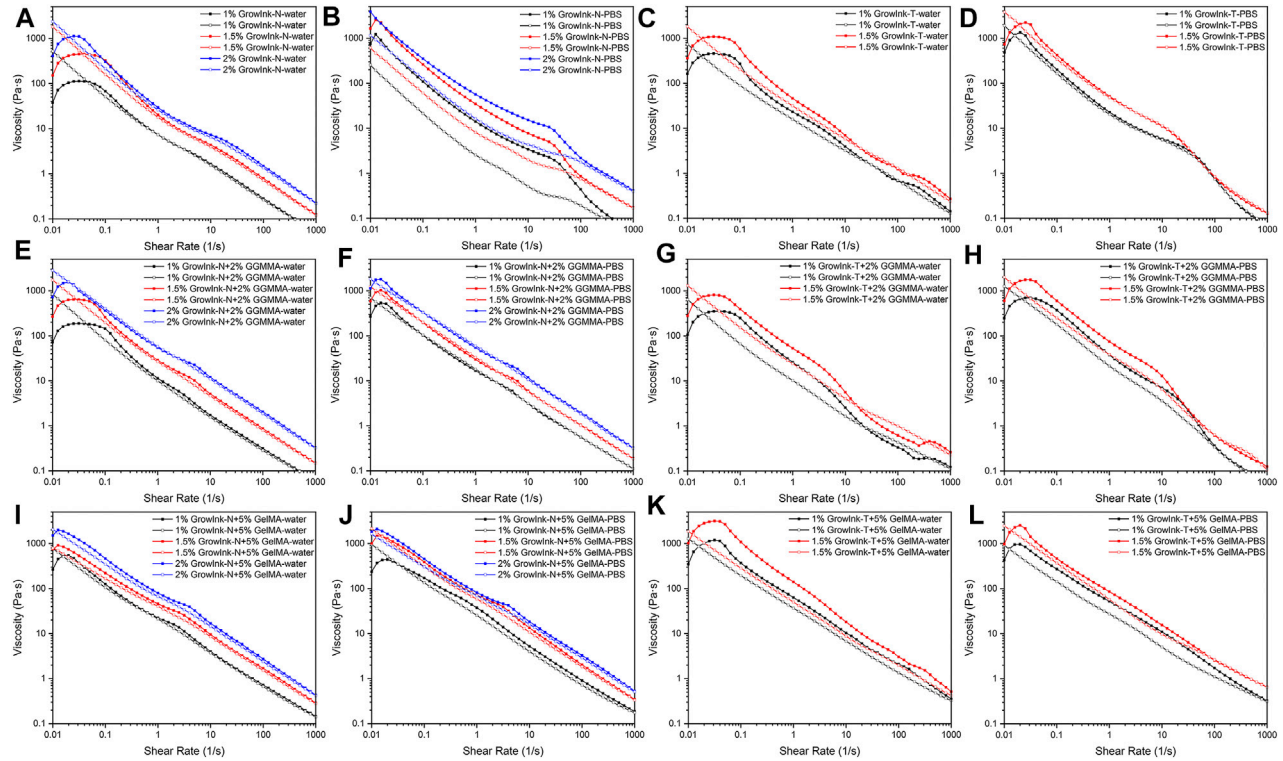

FIGURE 2 | Flow curves of formulated inks as a function of the shear rate [**(A–D)** GrowInk-N and GrowInk-T, **(E–H)** GGMMA incorporated GrowInk-N– and GrowInk-T–based inks, and **(I–L)** GelMA incorporated GrowInk-N– and GrowInk-T– based inks diluted with PBS buffer and water, respectively. Closed symbol: ramp-up and open symbol: ramp-down].

increase the inks' viscosity, owing to increased total mass content in the ink, as shown in **Figures 2E and I**.

In GrowInk-N, the entanglement of large-dimension nanofibrils dominates its gel-like structure. Whereas, the gel-like structure of GrowInk-T composed of relatively small-dimension nanofibrils is mainly governed by the strong fibril–fibril repulsion induced by its negatively charged surface groups (Benhamou et al., 2014). Therefore, the microstructure stability of GrowInk-T is more sensitive to the variation of ionic strength. As shown in **Figures 2C and D**, the electrostatic repulsion between nanofibrils in GrowInk-T was disordered by cations, causing the flocculation of CNFs. Therefore, GrowInk-T-PBS displayed a higher zero shear viscosity than GrowInk-T-water (Sim et al., 2015). As shown in **Figures 2G and H**, a similar trend in viscosity was observed in GrowInk-T-GGMMA–based inks. Similar to GrowInk-N-GelMA–based inks, the incorporation of GelMA greatly increased the viscosity of GrowInk-T-GelMA–based inks, as shown in **Figures 2K and L**. Moreover, the viscosity of GrowInk-T-GelMA–based inks was much higher than that of GrowInk-N-GelMA–based inks at the same concentration as shown in **Figures 2I and K**. This is mainly attributed to the ionic interaction between the positively charged GelMA and negatively charged GrowInk-T under neutral pH (Xu et al., 2019a).

Amplitude sweep is used to determine the linear viscoelastic region (LVER), which indicates the viscoelastic character of the test samples. The LVER is necessary to be registered prior to frequency sweep and photorheology. In addition, amplitude sweep could provide information such as yield stress (τ_y, the value of the shear stress at the limit of the LVER) and flow stress (τ_f, the value of the shear stress at the crossover point where G' equals G").

As shown in **Figures 3A and B**, G', τ_y, and τ_f of GrowInk-N-PBS increased drastically compared to the values of GrowInk-N-water. This is mainly due to the aggregation of CNFs flocs by the electrostatic screening effect as mentioned above. The τ_y and τ_f of 1.5% GrowInk-N-PBS were higher than that of 2% GrowInk-N-PBS. This might be due to higher ionic strength, leading to severe CNFs entanglement in 1.5% GrowInk-N-PBS, as a larger volume of PBS buffer was used in the preparation of 1.5% GrowInk-N-PBS than that used in 2% GrowInk-N-PBS. As shown in **Figures 3A and C**, G' of GrowInk-N-GGMMA inks was increased after incorporating GGMMA, whereas the τ_f was slightly increased. This indicates that the GGMMA could enhance the elasticity of the GrowInk-N–based ink without increasing its flow resistance. Meanwhile, G' and τ_f of GrowInk-N-GGMMA-PBS inks were decreased after incorporating GGMMA as shown in **Figures 3B and F**, except for 2% GrowInk-N + 2% GGMMA-PBS. This is because the steric stabilization effect of GGMMA could reduce the agglomeration effect and frictional interaction and thus leads to a lower τ_f (Araki et al., 2001). The steric stabilization effect of GGMMA could help prevent the aggregation of GrowInk-N CNFs flocs caused by cations, as shown in **Figures 3E and F**.

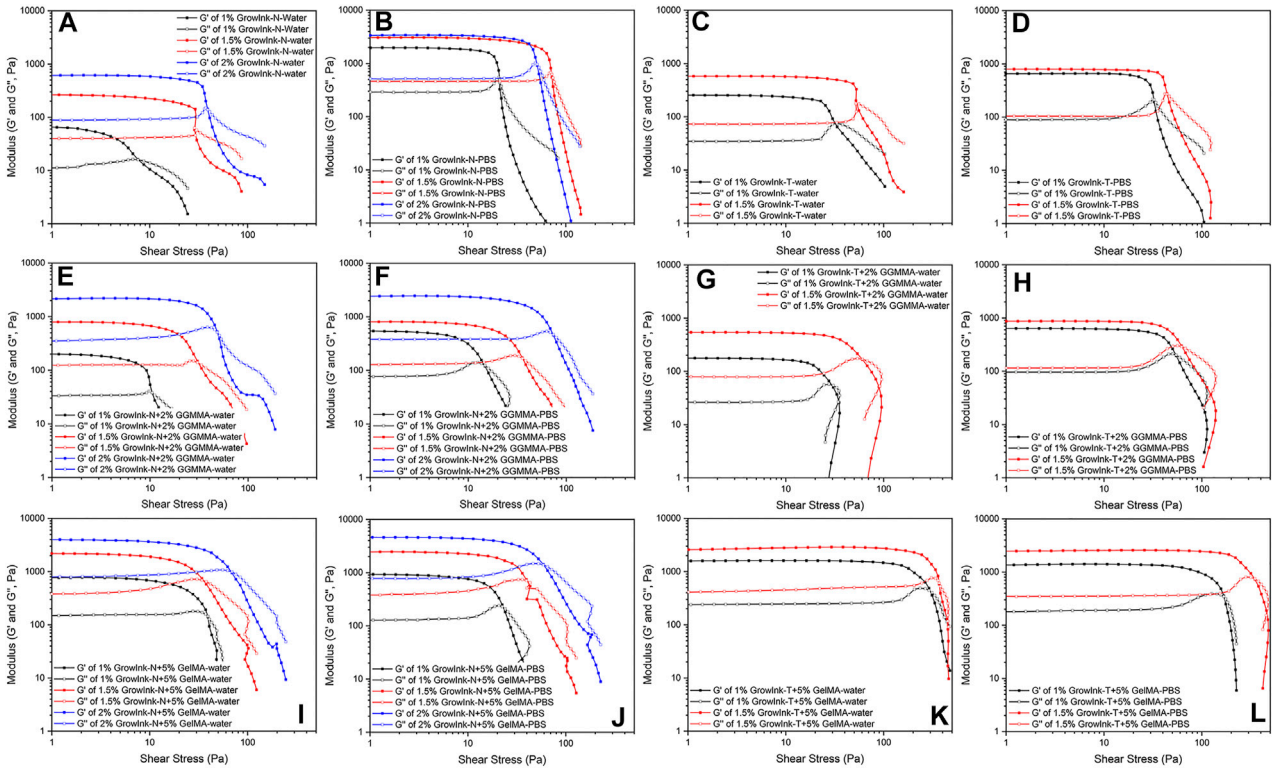

FIGURE 3 | Amplitude sweep of formulated inks plotted against the shear stress [**(A–D)** GrowInk-N and GrowInk-T, **(E–H)** GGMMA incorporated GrowInk-N and GrowInk-T, and **(I–L)** GelMA incorporated GrowInk-N– and GrowInk-T–based inks diluted with PBS buffer and water, respectively. Closed symbol: G' and open symbol: G"].

As shown in **Figures 3I and J**, incorporating 5% of GelMA in GrowInk-N significantly increases both G' and τ_f. Besides, the effect of PBS to GrowInk-N-GelMA–based inks was not significant on τ_f and G'. Except for the 1% GrowInk-N + 5% GelMA-PBS ink, τ_f was lower than that of the 1% GrowInk-N + 5% GelMA-water ink. It might be because the interactions between GelMA and GrowInk-N were disturbed under relatively higher ionic strength, and this resulted in a weaker microstructure maintenance ability with the imposed stress and strain. In addition, it is also indicated as shown in **Supplementary Figures S2I and J**, where the G" of 1% GrowInk-N + 5% GelMA-PBS ink displayed an apparent overshot at the end of the LVER compared to 1% GrowInk-N + 5% GelMA-water ink (Hyun et al., 2002).

As shown in **Figures 3A and C**, G' and τ_f of GrowInk-T-water were higher than those of GrowInk-N-water at the corresponding solid content level due to the strong electrostatic repulsion between nanofibrils. As shown in **Figures 3C and D**, G' and τ_f of GrowInk-T-PBS were increased in the absence of PBS buffer, which is similar to those of GrowInk-N. However, different from GrowInk-N-GGMMA inks, incorporation of GGMMA in GrowInk-T and GrowInk-T-PBS showed a limited effect on their G' and τ_f, as shown in **Figures 3G and H**. To be noticed, the flow transition index (τ_f/τ_y) of GrowInk-N and GrowInk-T was low, where the G' displayed a sudden drop at the end of the LVER, as shown in **Figures 3A–D**. However, the flow transition index was much higher after the incorporation of GGMMA, as shown in **Figures 3E–H**. This illustrates the structure transition of inks from the "brittle" to the "soft" material and demonstrates the effect of GGMMA on the viscoelastic property of CNFs-based inks (Corker et al., 2019). A similar phenomenon on the flow transition index was also observed in GrowInk-GelMA inks, as shown in **Figures 3I–L**. As shown in **Figures 3K and L**, the τ_f of the GrowInk-T-GelMA inks increased drastically, which is mainly attributed to the strong electrostatic interaction between GrowInk-T and GelMA. In addition, the τ_f of GrowInk-T-GelMA-PBS inks also displayed a decreased value when diluted with PBS buffer.

In light-aided, hydrogel extrusion–based 3D printing, the printing resolution is dictated by the shape maintenance ability of ink materials in between being extruded out of the needle and photo-curing. A viscosity recovery test is performed to monitor the viscosity change of the formulated inks post extrusion. A 3-stage shear test was adopted to mimic the applied shear rate on the inks and time scale during printing. In stage 1, a low shear rate of 0.1 s^{-1} was applied for 60 s to simulate at the rest condition. Following this, a high shear rate of 700 s^{-1} was applied immediately for 10 s to simulate the extrusion condition of the inks in the needle during printing in stage 2. The shear rate is calculated based on the printing condition of a printing speed of 12 mm/ s and an input flow rate of 100%. Then, a low shear rate of 0.1 s^{-1} was applied again to monitor the

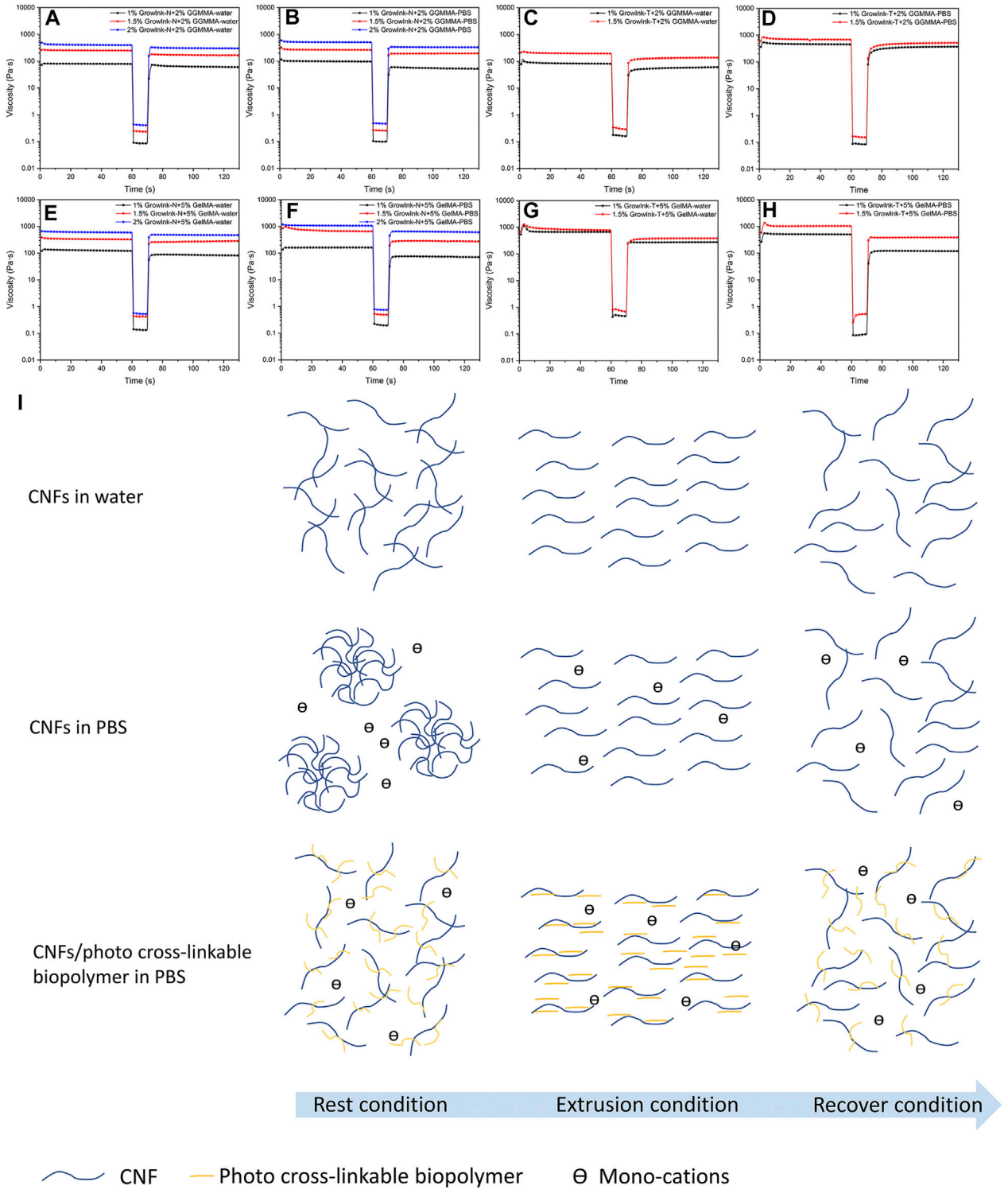

FIGURE 4 | Thixotropic behavior of the inks **(A–D)** GrowInk-N-GGMMA– and GrowInk-T-GGMMA–based inks, **(E–H)** GelMA incorporated GrowInk-N– and GrowInk-T–based inks diluted with PBS buffer and water, respectively, and **(I)** schematic illustration of the microstructure of the inks during the extrusion process. CNFs showed a stable microstructural network in water. The nanofibrils were orderly arranged during the extrusion condition and slowly recovered to a network structure after extrusion, whereas the CNFs in PBS buffer were aggregated into flocs at the rest condition and broke into individual nanofibrils during the extrusion process. The nanofibrils were not able to form into flocs immediately after extrusion. In contrast, the photo-crosslinkable polymer of GGMMA or GelMA absorbed on the surface of CNFs could significantly prevent floc formation, thus increasing the microstructure network stability during the extrusion process.

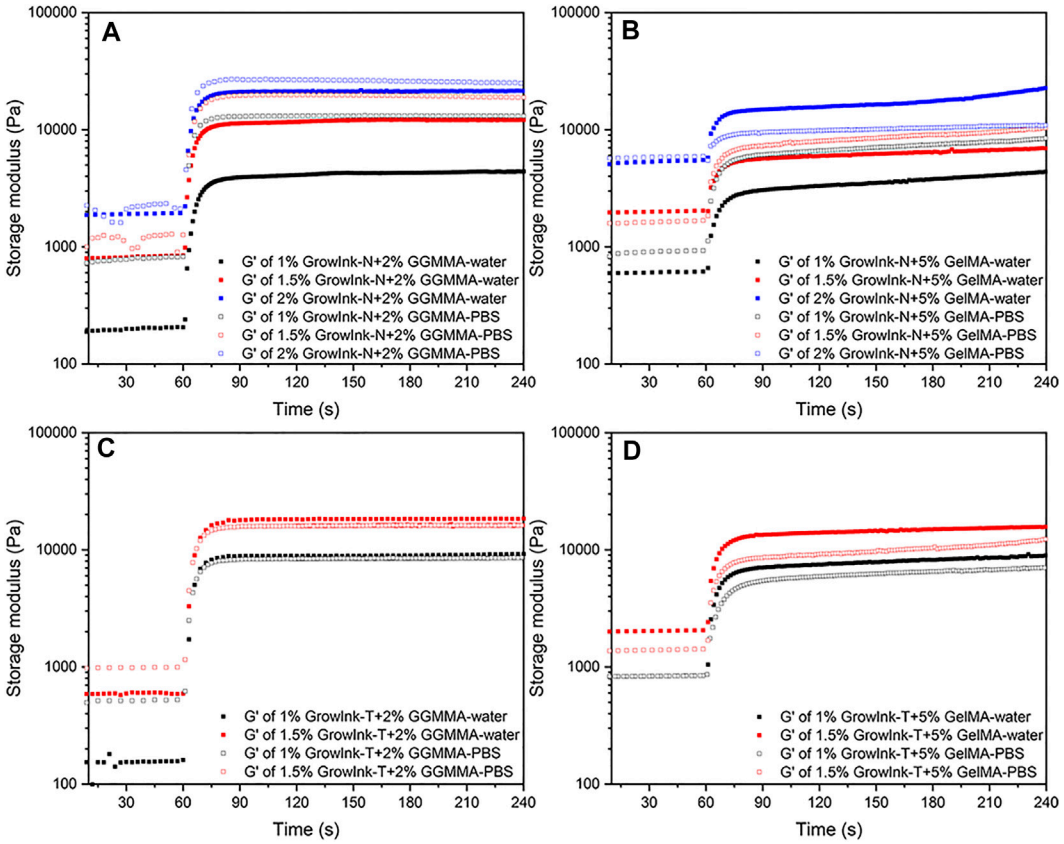

FIGURE 5 | Photorheology profiles of the formulated inks: **(A)** GrowInk-N-GGMMA–based inks, **(B)** GrowInk-N-GelMA–based inks, **(C)** GrowInk-T-GGMMA–based inks, and **(D)** GrowInk-T-GelMA–based inks diluted with PBS or water, respectively.

viscosity change of the inks after being extruded out of the needle. The viscosity recovery test was performed at 25°C to mimic the printability test performed in this study. As shown in **Figure 4**, all inks exhibited a fast recovery to stabilize viscosity with no lag observed within 10 s after a high shear rate. This suggests that the ink could maintain shape fidelity after extrusion in the process (Paxton et al., 2017). Meanwhile, the viscosity of all inks in stage 3 did not recover to the initial value in 60 s, indicating that their microstructure was changed. This is associated with the phenomenon in which randomly entangled CNFs at stage 1 were orderly arranged during high shear in stage 2, and the change would take longer to recover to the original state. As shown in **Figure 4**, the viscosity recovery ability of GrowInk-GelMA inks was more vulnerable to PBS than GrowInk-GGMMA inks. This might be owing to the monovalent cation in PBS that disordered the electrostatic repulsion between CNFs and GelMA, thus leading to difficult recovery phase-separated at a high shear rate.

For hydrogel extrusion–based 3D printing, efficient crosslinking of ink materials is the key to achieve good shape fidelity. Rapid and robust crosslinking of the extruded filament is demanded to support the layer-by-layer fabrication of printed 3D objects in complex structures and to prevent distortion against gravity. In our study, photo-crosslinkable GGMMA or GelMA was formulated together with GrowInk to facilitate the covalent crosslinking of the interpenetrating polymer networks with UV irradiation. Photo-rheology was applied to monitor the photo-crosslinking kinetics of the inks, and the G' was recorded upon kicking off the UV irradiation. Theoretically, a minimum G' of 2.15 kPa to support an extruded filament span over a distance 5 times larger than the nozzle diameter can be established using a simple beam theory with the following equation:

$$G^{'} \geq 1.4\gamma s^4 D \tag{3}$$

where γ is the specific weight of the ink, s is the span distance (=L/D), L is the span width, and D is the nozzle diameter. The acceptable deflection is 0.05D (Smay et al., 2002; Schaffner et al., 2017).

As shown in **Figure 5**, maximum G' (G'_{max}) increased with the increase in CNFs content within inks with the same content of GGMMA or GelMA. The G' of all inks was increased dramatically upon UV irradiation. The G'_{max} of all inks was higher than 2.15 kPa, and the required time of G' to exceed 2.15 kPa is summarized in **Supplementary Table S2**. As shown in **Figures 5A and B**, the G'_{max} of most GrowInk-N-PBS-based inks was higher than that of GrowInk-N-water–based inks, except 2% GrowInk-N + 5% GelMA, whereas the G'_{max} of GrowInk-N-PBS–based inks was lower than that of GrowInk-T-water–based inks, as shown in **Figures 5C and D**.

Printability Assessment

Rheological measurements are performed with the given measuring parameters to mimic the ink flow conditions of the printing process. These measurements could provide quantitative information on the viscosity, viscoelastic properties, recovery behavior, and photo-crosslinking kinetics of the inks. However, the rheological simulation could not perfectly reproduce the printing process, and the rheological evaluation could not define the absolute criteria for printability (Paxton et al., 2017). Therefore, comprehensive printability assessments are required to provide essential information for adapting new ink formulations in hydrogel extrusion–based 3D printing. Considering the practical scenario of saline introduced by cell-mixing in 3D bioprinting, the printability was mainly evaluated for the GrowInk-based inks diluted with PBS. However, as we often experienced clogging in the needle when printing GrowInk-T-PBS–based inks, the printability was evaluated for the GrowInk-T–based inks diluted with water. Electrostatic repulsion between GrowInk-T CNFs contributes to their gel-like structure and desired viscoelasticity, as revealed in rheological studies. Meanwhile, it also determines that the colloidal stability of GrowInk-T is sensitive to ionic strength when diluted with PBS.

Extrudability is the ability to produce uniform and continuous filaments under given printing conditions, which is the fundamental requirement in extrusion-based 3D printing. In the extrudability analysis, the printing speed and the input flow rate were controlled, and the uniformity ratio and width of the printed filaments were evaluated. As shown in **Supplementary Figure S3A**, the filaments of GrowInk-N-GGMMA-PBS inks displayed a smooth outline and the uniformity ratio was not dependent on the GrowInk-N loading, printing speed, and input flow rate. In contrast, the uniformity ratio of GrowInk-T-GGMMA-water inks increased with the increase in printing speed and decreased with the increase of GrowInk-T loading. As shown in **Supplementary Figure S3C**, both GrowInk-N-GelMA-PBS and GrowInk-T-GelMA-water inks displayed quite good uniformity regardless of the printing speed, input flow ratio, and CNF loading.

The width of the filament indicates its ability to hold a cylindrical shape and also against spreading. As shown in **Supplementary Figures S3B and D**, the overall filament width decreased with the increase of the GrowInk-N and GrowInk-T loading, attributed to the increasing G' and crosslinking kinetics. Due to the difference in the physicochemical properties of the photo-crosslinkable polymer, GrowInk-N–based inks incorporated with GGMMA or GelMA behaved differently under the same extrusion condition. The filament width of GrowInk-N-GGMMA-PBS inks decreased with the increase in printing speed under the same input flow, but the filament width of GrowInk-N-GelMA-PBS inks increased with the increase in the input flow rate, as shown in **Supplementary Figure S3D**. Meanwhile, the GrowInk-T-GelMA-water inks displayed an outstanding performance against spreading. This might be attributed to the strong interaction between GrowInk-T and GelMA, besides the relatively higher G' and faster crosslinking kinetics. Speaking of the printing resolution as defined by both the filament width and uniformity, 1.5 and 2% GrowInk-N + 2% GGMMA-PBS inks and 1% GrowInk-T+5% GelMA-water ink allowed a decent printing resolution of uniform filaments less than 500 μm. Based on the extrudability evaluation and aiming to decrease shear stress at the needle, a printing speed of 12 m/ s was applied in the following printability assessment by printing layer-by-layer cross-hatch scaffolds.

When printing a cross-hatch scaffold with an ideally gelated ink, the outcome pores would display a square shape (Ouyang et al., 2016). A Pr value was developed to quantify filament uniformity and gelation condition by comparing the circularity of the outcome pore to a perfectly square pore (Ouyang et al., 2016). However, in practice, the gel-like behaviour of the printed filament would lead to fusion between the stacking filaments, especially for inks with an under-gelation status. Thus, the outcome square pores would display varying degrees of circularity. As observed in **Figure 6**, all inks displayed an under-gelation status under different printing conditions, in which the Pr values were in the range from 0.8 to 1.0. In this case, the diffusion rate (Dr) value should also be considered to evaluate their printability because filament spreading would also lead to printing failure by losing printing accuracy. As observed in **Figures 6D and E**, the Pr values did not display a noticeable difference between the two scaffolds of 1.5% GrowInk-N + 5% GelMA-PBS that were printed with a constant layer height of 0.07 mm but at different input flow rates; however, the filament spreading resulted in almost closure of pores in the grid as the input flow increased. Hence, the Dr value was carried out to evaluate the pore closure effect caused by filament spreading during the printing by comparing the outcome pore area with its theoretical area (Habib et al., 2018). These two factors could quantitatively evaluate the printability of the inks. In this study, 10-layer cross-hatch scaffolds were printed under the given printing conditions for the ink formulations that showed promising extrudability. As shown in **Figure 6**, Dr values increased with the increase in the input flow rate for the same formulation, which indicated a more severe spreading of the filaments and closure of the pore. Meanwhile, Dr values decreased with an increase in the layer height. The filaments of under-gelation inks are not likely to hold an ideal cylindrical structure. Thus, the layer height should be considered and adjusted to reach an acceptable resolution.

To further analyze the printability of inks and evaluate the structural stability of printed objects, 36-layer scaffolds were printed under the printing parameter set at a layer height of 0.09 mm and input flow rate of 100% and were further incubated in PBS buffer and DMEM for 7 days, respectively. As shown in **Figure 7**, all scaffolds displayed a good height maintenance ability, and no apparent collapse was observed. Subsequently, the printed scaffolds were incubated in PBS and DMEM to evaluate their structural stability in the cell culture medium. All scaffolds displayed structural integrity, where no apparent contraction and swelling was observed after 7 days.

Mechanical Property

The mechanical property of hydrogel scaffolds is one of the vital aspects considering its application in the biomaterials field. As

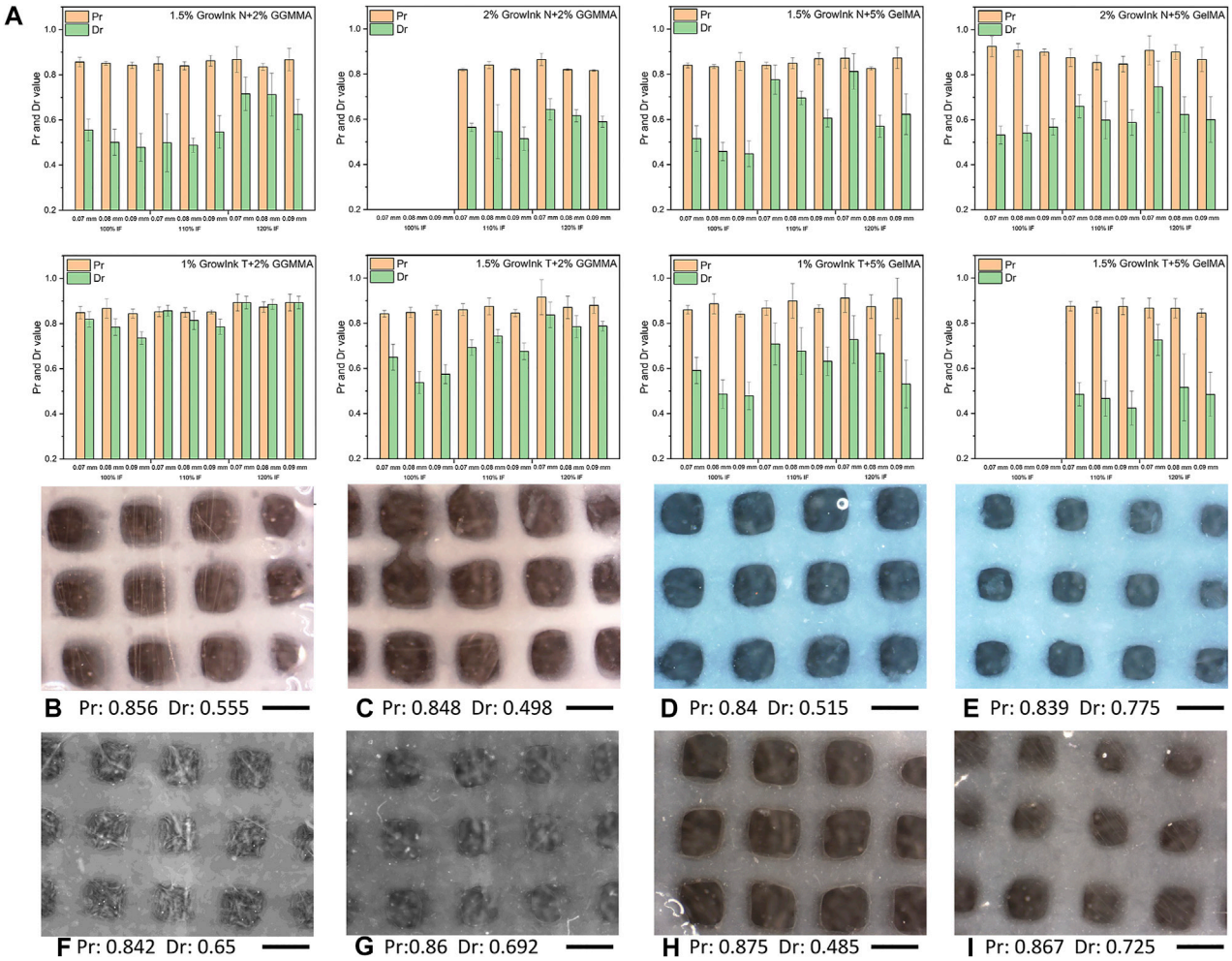

FIGURE 6 | (A) Pr and Dr values and (B–I) optical microscope images of the cross-hatch scaffold printed with formulated inks under different printing parameters: **(B and C)** printed with 1.5% GrowInk-N + 2% GGMMA-PBS with a layer height of 0.07 mm and an input flow rate of 100 and 110%, respectively, **(D and E)** printed with 1.5% GrowInk-N+5% GelMA-PBS with a layer height of 0.07 mm and an input flow rate of 100 and 110%, respectively, **(F and G)** printed with 1.5% GrowInk-T + 2% GGMMA-PBS with a layer height of 0.07 mm and an input flow rate of 100 and 110%, respectively, **(H and I)** printed with 1.5% GrowInk-T + 5% GelMA-PBS with a layer height of 0.07 mm and an input flow rate of 110 and 120%, respectively. Scale bar: 1 mm)

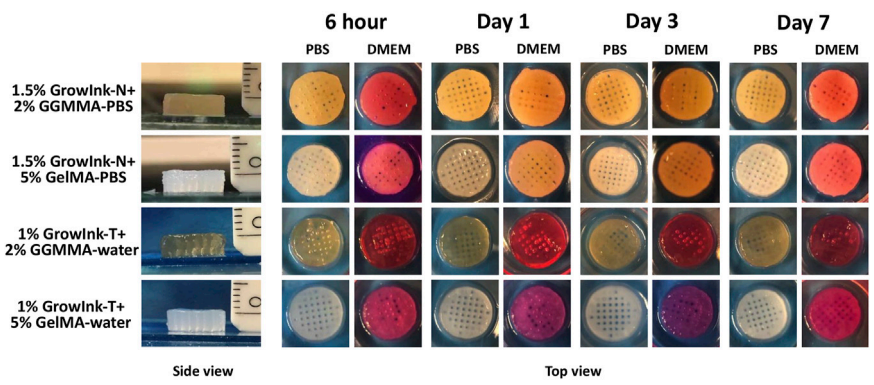

FIGURE 7 | Side and top views of the printed hydrogel scaffolds incubated in PBS buffer and DMEM for 7 days.

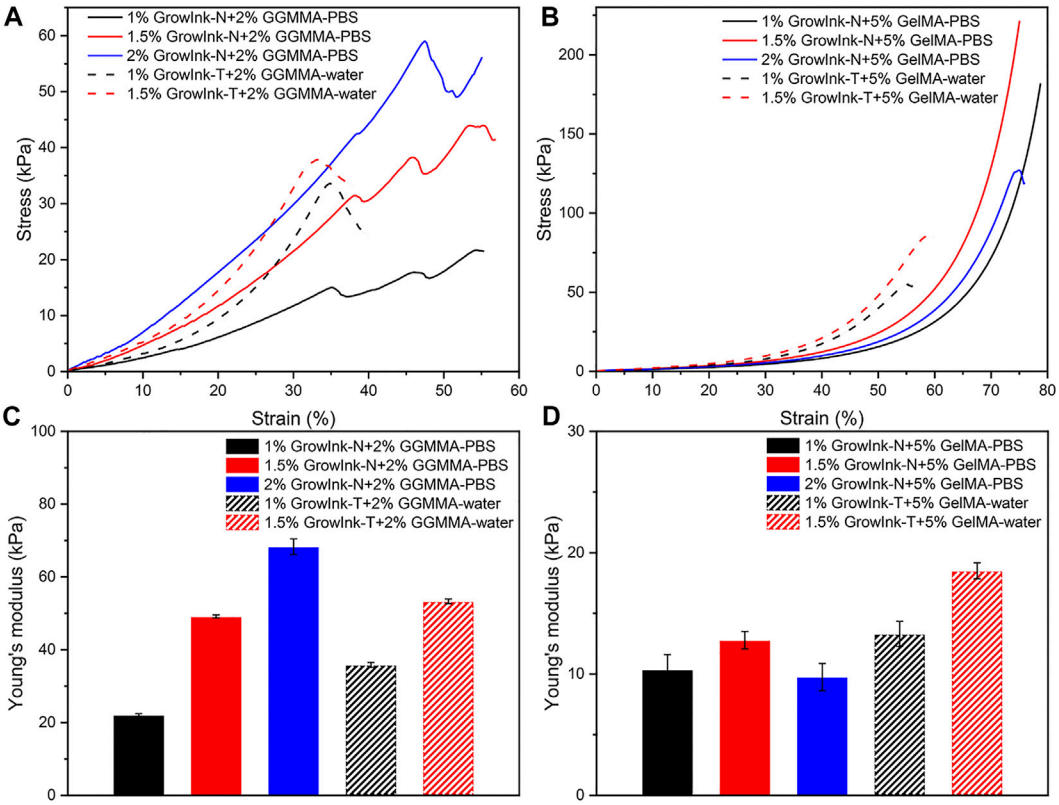

FIGURE 8 | Compressive stress–strain curves and compressive Young's modulus of hydrogels fabricated by GrowInk-N and T with **(A and C)** GGMMA and **(B and D)** GelMA.

shown in **Figures 8A and C**, Young's modulus and the yield strain of the GrowInk-GGMMA–based hydrogels increased with the increase of the CNF loading. In addition, Young's modulus of the GrowInk-T-GGMMA–based hydrogels was higher than that of the GrowInk-N-GGMMA–based hydrogels for the same CNF loading, whereas the fracture strain of the GrowInk-T-GGMMA–based hydrogels was slightly smaller than that of the GrowInk-N-GGMMA–based hydrogels. This indicated a stiffer and more brittle mechanical property of the GrowInk-T-GGMMA–based hydrogels. More likely, the small and surface-charged GrowInk-T-CNFs could evenly disperse in GGMMA and form a comparatively homogeneous hydrogel than the GrowInk-N-GGMMA–based ink (Takeno et al., 2020). A similar trend in Young's modulus could also be observed in the GrowInk-GelMA–based hydrogels, as shown in **Figures 8B and D**. Unexpectedly, the hydrogel of 2% GrowInk-N + 5% GelMA-PBS displayed a drop in Young's modulus compared to the hydrogel of 1.5% GrowInk-N + 5% GelMA-PBS. This might be because the high solid loading of GrowInk-N inhibited the crosslinking of GelMA, leading to a lower crosslinking density. Meanwhile, the yield strain of GrowInk-N–based hydrogels was higher than that of the GrowInk-T–based hydrogels, as shown in **Figures 8A and B**. It is inferred that the CNFs in the GrowInk-N hydrogel are entangled to a more significant extent, which facilitates energy dissipation. Besides, Young's modulus of the GelMA-based hydrogels is much lower than that of the GGMMA-based hydrogels. One aspect to account for is the relatively lower DM of GelMA than GGMMA, which leads to a lower crosslinking density and softer structure. The result of Young's modulus is in line with the G' in photo-rheology. Overall, Young's modulus of the hydrogel disks is tunable in a wide range from 9.35 to 68.32 kPa.

CONCLUSION

When CNFs are used as a major constituent in formulating biomaterial inks with a photo-crosslinkable biopolymer, the nanodimensions of and the surface charge on CNFs together dominate the rheological properties of the as-prepared nanocellulose-based inks and, consequently, dictate the ink printability in light-aided, hydrogel-extrusion–based 3D printing. On using PBS buffer as the formulation medium, the gel structure of TEMPO-oxidized CNFs-based inks (GrowInk-T–based ink) is sensitive to the variation of ionic strength, which would potentially make complex its application in cell-laden 3D bioprinting. Owing to the specific absorption of GGMMA onto CNFs *via* hydrogen bonding, the addition of 2% GGMMA in GrowInk-N diminished the hysteresis behavior of the GrowInk-N-PBS ink by preventing the formation of uneven

microstructures of flocs upon variation of ionic strength. Furthermore, the addition of 2% GGMMA significantly decreased the G' value and the flow stress. In comparison, the addition of 5% GelMA in GrowInk-T largely increased the flow stress because of the electrostatic interaction between GelMA and TEMPO-oxidized CNFs. With the same content of CNFs, 2% GGMMA-containing inks exhibited faster crosslinking kinetics and resulted in stiffer hydrogels than 5% GelMA-containing inks because of their high DM and intrinsic absorption onto nanofibrils. Meanwhile, the GelMA-containing hydrogels were soft but more elastic, which showed an extended strain at break. Compared to GrowInk-T–based inks, the GrowInk-N–based inks with the addition of either GGMMA or GelMA in PBS buffer showed quite good printability on optimizing the printing parameters. Upon UV-crosslinking, the printed scaffolds displayed an under-gelation status and the Dr value was more significant in the printability assessment than the Pr value. The shape fidelity of the formulated inks is mainly determined by the input flow rate, layer height, and CNFs concentration.

DATA AVAILABILITY STATEMENT

The original contributions presented in the study are included in the article/**Supplementary Material**; further inquiries can be directed to the corresponding author.

AUTHOR CONTRIBUTIONS

All authors contributed to the experimental design, planning, execution, and data analysis. QW and OB carried out the main experimental work. QW and XW drafted the original draft manuscript. MN and CX provided critical revision to the manuscript. XW is the main scientist who supervised the work. The manuscript has been approved by all the co-authors for submission.

FUNDING

QW was supported by the research grants from the China Scholarship Council (Student ID 201907960002) and KAUTE Foundation (Project number 20190031) at Abo Akademi University (AAU), Finland. The major sponsor of research resources used in the current research is the Academy of Finland (AoF) (333158). The AoF project has received funds for its open access publication fee.

ACKNOWLEDGMENTS

QW would like to acknowledge the financial support from the China Scholarship Council (Student ID 201907960002) and KAUTE Foundation (Project number 20190031) to his doctoral study at Abo Akademi University (ÅAU), Finland. XW would like to thank the Academy of Finland (333158) as well as Jane and Aatos Erkko Foundation for their funds to her research at AAU. This work is also part of activities within the Johan Gadolin Process Chemistry Centre (PCC) at AAU. Luyao Wang is gratefully acknowledged for assisting the TEM analysis.

SUPPLEMENTARY MATERIAL

The Supplementary Material for this article can be found online at: https://www.frontiersin.org/articles/10.3389/fceng.2021.723429/full#supplementary-material

REFERENCES

Ajdary, R., Huan, S., Zanjanizadeh Ezazi, N., Xiang, W., Grande, R., Santos, H. A., et al. (2019). Acetylated Nanocellulose for Single-Component Bioinks and Cell Proliferation on 3D-Printed Scaffolds. *Biomacromolecules* 20, 2770–2778. doi:10.1021/acs.biomac.9b00527

Araki, J., Wada, M., and Kuga, S. (2001). Steric Stabilization of a Cellulose Microcrystal Suspension by Poly(ethylene Glycol) Grafting. *Langmuir* 17, 21–27. doi:10.1021/la001070m

Benhamou, K., Dufresne, A., Magnin, A., Mortha, G., and Kaddami, H. (2014). Control of Size and Viscoelastic Properties of Nanofibrillated Cellulose from palm Tree by Varying the TEMPO-Mediated Oxidation Time. *Carbohydr. Polym.* 99, 74–83. doi:10.1016/j.carbpol.2013.08.032

Chinga-Carrasco, G., Averianova, N., Kondalenko, O., Garaeva, M., Petrov, V., Leinsvang, B., et al. (2014). The Effect of Residual Fibres on the Micro-topography of Cellulose Nanopaper. *Micron* 56, 80–84. doi:10.1016/j.micron.2013.09.002

Claaßen, C., Claaßen, M. H., Truffault, V., Sewald, L., Tovar, G. E. M., Borchers, K., et al. (2018). Quantification of Substitution of Gelatin Methacryloyl: Best Practice and Current Pitfalls. *Biomacromolecules* 19, 42–52. doi:10.1021/acs.biomac.7b01221

Corker, A., Ng, H. C.-H., Poole, R. J., and García-Tuñón, E. (2019). 3D Printing with 2D Colloids: Designing Rheology Protocols to Predict 'printability' of Soft-Materials. *Soft Matter* 15, 1444–1456. doi:10.1039/c8sm01936c

Engler, A. J., Sen, S., Sweeney, H. L., and Discher, D. E. (2006). Matrix Elasticity Directs Stem Cell Lineage Specification. *Cell* 126, 677–689. doi:10.1016/j.cell.2006.06.044

Fan, Y., Yue, Z., Lucarelli, E., and Wallace, G. G. (2020). Hybrid Printing Using Cellulose Nanocrystals Reinforced GelMA/HAMA Hydrogels for Improved Structural Integration. *Adv. Healthc. Mater.* 9, 2001410. doi:10.1002/adhm.202001410

Fukuzumi, H., Tanaka, R., Saito, T., and Isogai, A. (2014). Dispersion Stability and Aggregation Behavior of TEMPO-Oxidized Cellulose Nanofibrils in Water as a Function of Salt Addition. *Cellulose* 21, 1553–1559. doi:10.1007/s10570-014-0180-z

Gao, T., Gillispie, G. J., Copus, J. S., Pr, A. K., Seol, Y.-J., Atala, A., et al. (2018). Optimization of Gelatin-Alginate Composite Bioink Printability Using Rheological Parameters: A Systematic Approach. *Biofabrication* 10, 034106. doi:10.1088/1758-5090/aacdc7

Gillispie, G., Prim, P., Copus, J., Fisher, J., Mikos, A. G., Yoo, J. J., et al. (2020). Assessment Methodologies for Extrusion-Based Bioink Printability. *Biofabrication* 12, 022003. doi:10.1088/1758-5090/ab6f0d

Habib, A., Sathish, V., Mallik, S., and Khoda, B. (2018). 3D Printability of Alginate-Carboxymethyl Cellulose Hydrogel. *Materials* 11, 454. doi:10.3390/ma11030454

Heggset, E. B., Strand, B. L., Sundby, K. W., Simon, S., Chinga-Carrasco, G., and Syverud, K. (2019). Viscoelastic Properties of Nanocellulose Based Inks for 3D Printing and Mechanical Properties of CNF/alginate Biocomposite Gels. *Cellulose* 26, 581–595. doi:10.1007/s10570-018-2142-3

Hinton, T. J., Jallerat, Q., Palchesko, R. N., Park, J. H., Grodzicki, M. S., Shue, H.-J., et al. (2015). Three-dimensional Printing of Complex Biological Structures by Freeform Reversible Embedding of Suspended Hydrogels. *Sci. Adv.* 1, e1500758. doi:10.1126/sciadv.1500758

Huang, L., Yuan, W., Hong, Y., Fan, S., Yao, X., Ren, T., et al. (2020). 3D Printed Hydrogels with Oxidized Cellulose Nanofibers and Silk Fibroin for the Proliferation of Lung Epithelial Stem Cells. *Cellulose* 28, 241–257. doi:10.1007/s10570-020-03526-7

Hubbe, M. A., Tayeb, P., Joyce, M., Tyagi, P., Kehoe, M., Dimic-Misic, K., et al. (2017). Rheology of Nanocellulose-Rich Aqueous Suspensions: A Review. *BioRes* 12, 9556–9661. Available at: https://ojs.cnr.ncsu.edu/index.php/BioRes/article/view/BioRes_12_4_9556_Hubbe_Rheology_Nanocellulose_Aqueous_Suspension/5699. doi:10.15376/biores.12.4.hubbe

Hyun, K., Kim, S. H., Ahn, K. H., and Lee, S. J. (2002). Large Amplitude Oscillatory Shear as a Way to Classify the Complex Fluids. *J. Non-Newtonian Fluid Mech.* 107, 51–65. doi:10.1016/S0377-0257(02)00141-6

Kang, H.-W., Lee, S. J., Ko, I. K., Kengla, C., Yoo, J. J., and Atala, A. (2016). A 3D Bioprinting System to Produce Human-Scale Tissue Constructs with Structural Integrity. *Nat. Biotechnol.* 34, 312–319. doi:10.1038/nbt.3413

Levanič, J., Šenk, V. P., Nadrah, P., Poljanšek, I., Oven, P., and Haapala, A. (2020). Analyzing TEMPO-Oxidized Cellulose Fiber Morphology: New Insights into Optimization of the Oxidation Process and Nanocellulose Dispersion Quality. *ACS Sustain. Chem. Eng.* 8, 17752–17762. doi:10.1021/acssuschemeng.0c05989

Lewis, P. L., Green, R. M., and Shah, R. N. (2018). 3D-printed Gelatin Scaffolds of Differing Pore Geometry Modulate Hepatocyte Function and Gene Expression. *Acta Biomater.* 69, 63–70. doi:10.1016/j.actbio.2017.12.042

Li, V. C. F., Mulyadi, A., Dunn, C. K., Deng, Y., and Qi, H. J. (2018). Direct Ink Write 3D Printed Cellulose Nanofiber Aerogel Structures with Highly Deformable, Shape Recoverable, and Functionalizable Properties. *ACS Sust. Chem. Eng.* 6, 2011–2022. doi:10.1021/acssuschemeng.7b03439

Lim, K. S., Galarraga, J. H., Cui, X., Lindberg, G. C. J., Burdick, J. A., and Woodfield, T. B. F. (2020). Fundamentals and Applications of Photo-Cross-Linking in Bioprinting. *Chem. Rev.* 120, 10662–10694. doi:10.1021/acs.chemrev.9b00812

Lou, Y.-R., Kanninen, L., Kuisma, T., Niklander, J., Noon, L. A., Burks, D., et al. (2014). The Use of Nanofibrillar Cellulose Hydrogel as a Flexible Three-Dimensional Model to Culture Human Pluripotent Stem Cells. *Stem Cell Dev.* 23, 380–392. doi:10.1089/scd.2013.0314

Ma, Q., Mohawk, D., Jahani, B., Wang, X., Chen, Y., Mahoney, A., et al. (2020). UV-curable Cellulose Nanofiber-Reinforced Soy Protein Resins for 3D Printing and Conventional Molding. *ACS Appl. Polym. Mater.* 2, 4666–4676. doi:10.1021/acsapm.0c00717

Markstedt, K., Mantas, A., Tournier, I., Martínez Ávila, H., Hägg, D., and Gatenholm, P. (2015). 3D Bioprinting Human Chondrocytes with Nanocellulose-Alginate Bioink for Cartilage Tissue Engineering Applications. *Biomacromolecules* 16, 1489–1496. doi:10.1021/acs.biomac.5b00188

Nechyporchuk, O., Belgacem, M. N., and Bras, J. (2016). Production of Cellulose Nanofibrils: A Review of Recent Advances. *Ind. Crops Prod.* 93, 2–25. doi:10.1016/j.indcrop.2016.02.016

O'Brien, F. J. (2011). Biomaterials & Scaffolds for Tissue Engineering. *Mater. Today* 14, 88–95. doi:10.1016/S1369-7021(11)70058-X

Oh, K., Kwon, S., Xu, W., Wang, X., and Toivakka, M. (2020). Effect of Micro- and Nanofibrillated Cellulose on the Phase Stability of Sodium Sulfate Decahydrate Based Phase Change Material. *Cellulose* 27, 5003–5016. doi:10.1007/s10570-020-03121-w

Ojansivu, M., Rashad, A., Ahlinder, A., Massera, J., Mishra, A., Syverud, K., et al. (2019). Wood-based Nanocellulose and Bioactive Glass Modified Gelatin-Alginate Bioinks for 3D Bioprinting of Bone Cells. *Biofabrication* 11, 035010. doi:10.1088/1758-5090/ab0692

Ouyang, L., Yao, R., Zhao, Y., and Sun, W. (2016). Effect of Bioink Properties on Printability and Cell Viability for 3D Bioplotting of Embryonic Stem Cells. *Biofabrication* 8, 035020. doi:10.1088/1758-5090/8/3/035020

Paxton, N., Smolan, W., Böck, T., Melchels, F., Groll, J., and Jungst, T. (2017). Proposal to Assess Printability of Bioinks for Extrusion-Based Bioprinting and Evaluation of Rheological Properties Governing Bioprintability. *Biofabrication* 9, 044107. doi:10.1088/1758-5090/aa8dd8

Rees, A., Powell, L. C., Chinga-Carrasco, G., Gethin, D. T., Syverud, K., Hill, K. E., et al. (2015). 3D Bioprinting of Carboxymethylated-Periodate Oxidized Nanocellulose Constructs for Wound Dressing Applications. *Biomed. Res. Int.* 2015, 1–7. doi:10.1155/2015/925757

Rhee, S., Puetzer, J. L., Mason, B. N., Reinhart-King, C. A., and Bonassar, L. J. (2016). 3D Bioprinting of Spatially Heterogeneous Collagen Constructs for Cartilage Tissue Engineering. *ACS Biomater. Sci. Eng.* 2, 1800–1805. doi:10.1021/acsbiomaterials.6b00288

Saarikoski, E., Saarinen, T., Salmela, J., and Seppälä, J. (2012). Flocculated Flow of Microfibrillated Cellulose Water Suspensions: An Imaging Approach for Characterisation of Rheological Behaviour. *Cellulose* 19, 647–659. doi:10.1007/s10570-012-9661-0

Schaffner, M., Rühs, P. A., Coulter, F., Kilcher, S., and Studart, A. R. (2017). 3D Printing of Bacteria into Functional Complex Materials. *Sci. Adv.* 3, eaao6804. doi:10.1126/sciadv.aao6804

Shin, S., Park, S., Park, M., Jeong, E., Na, K., Youn, H. J., et al. (2017). Cellulose Nanofibers for the Enhancement of Printability of Low Viscosity Gelatin Derivatives. *BioResources* 12, 2941–2954. doi:10.15376/biores.12.2.2941-2954

Sim, K., Lee, J., Lee, H., and Youn, H. J. (2015). Flocculation Behavior of Cellulose Nanofibrils under Different Salt Conditions and its Impact on Network Strength and Dewatering Ability. *Cellulose* 22, 3689–3700. doi:10.1007/s10570-015-0784-y

Smay, J. E., Cesarano, J., and Lewis, J. A. (2002). Colloidal Inks for Directed Assembly of 3-D Periodic Structures. *Langmuir* 18, 5429–5437. doi:10.1021/la0257135

Takeno, H., Inoguchi, H., and Hsieh, W.-C. (2020). Mechanical and Structural Properties of Cellulose Nanofiber/poly(vinyl Alcohol) Hydrogels Cross-Linked by a Freezing/thawing Method and Borax. *Cellulose* 27, 4373–4387. doi:10.1007/s10570-020-03083-z

Winter, H. T., Cerclier, C., Delorme, N., Bizot, H., Quemener, B., and Cathala, B. (2010). Improved Colloidal Stability of Bacterial Cellulose Nanocrystal Suspensions for the Elaboration of Spin-Coated Cellulose-Based Model Surfaces. *Biomacromolecules* 11, 3144–3151. doi:10.1021/bm100953f

Xu, C., Zhang Molino, B., Wang, X., Cheng, F., Xu, W., Molino, P., et al. (2018a). 3D Printing of Nanocellulose Hydrogel Scaffolds with Tunable Mechanical Strength towards Wound Healing Application. *J. Mater. Chem. B.* 6, 7066–7075. doi:10.1039/c8tb01757c

Xu, W., Molino, B. Z., Cheng, F., Molino, P. J., Yue, Z., Su, D., et al. (2019a). On Low-Concentration Inks Formulated by Nanocellulose Assisted with Gelatin Methacrylate (GelMA) for 3D Printing toward Wound Healing Application. *ACS Appl. Mater. Inter.* 11, 8838–8848. doi:10.1021/acsami.8b21268

Xu, W., Zhang, X., Yang, P., Långvik, O., Wang, X., Zhang, Y., et al. (2019b). Surface Engineered Biomimetic Inks Based on UV Cross-Linkable Wood Biopolymers for 3D Printing. *ACS Appl. Mater. Inter.* 11, 12389–12400. doi:10.1021/acsami.9b03442

Xu, X., Zhou, J., Jiang, Y., Zhang, Q., Shi, H., and Liu, D. (2018b). 3D Printing Process of Oxidized Nanocellulose and Gelatin Scaffold. *J. Biomater. Sci. Polym. Edition.* 29, 1498–1513. doi:10.1080/09205063.2018.1472450

Yang, X., Lu, Z., Wu, H., Li, W., Zheng, L., and Zhao, J. (2018). Collagen-alginate as Bioink for Three-Dimensional (3D) Cell Printing Based Cartilage Tissue Engineering. *Mater. Sci. Eng. C.* 83, 195–201. doi:10.1016/j.msec.2017.09.002

Conflict of Interest: Author MN was employed by the company UPM-Kymmene Comporation, Biomedicals.

The remaining authors declare that the research was conducted in the absence of any commercial or financial relationships that could be construed as a potential conflict of interest.

Publisher's Note: All claims expressed in this article are solely those of the authors and do not necessarily represent those of their affiliated organizations, or those of the publisher, the editors and the reviewers. Any product that may be evaluated in this article, or claim that may be made by its manufacturer, is not guaranteed or endorsed by the publisher.